HAL
open science

Full potential x-ray absorption calculations using the time dependent density functional theory

Oana Bunau, Yves Joly

To cite this version:

Oana Bunau, Yves Joly. Full potential x-ray absorption calculations using the time dependent density functional theory. Journal of Physics: Condensed Matter, 2012, 24, pp.215502. 10.1088/0953-8984/24/21/215502 . hal-00691360

HAL Id: hal-00691360

https://hal.science/hal-00691360v1

Submitted on 26 Apr 2012

HAL is a multi-disciplinary open access archive for the deposit and dissemination of scientific research documents, whether they are published or not. The documents may come from teaching and research institutions in France or abroad, or from public or private research centers.

L'archive ouverte pluridisciplinaire **HAL**, est destinée au dépôt et à la diffusion de documents scientifiques de niveau recherche, publiés ou non, émanant des établissements d'enseignement et de recherche français ou étrangers, des laboratoires publics ou privés.

Full Potential X-ray Absorption Calculations Using the Time Dependent Density Functional Theory

O. Bunău[1] ‡ **and Y. Joly**[1]

[1] Institut Néel - 25 rue de Martyrs, 38042 Grenoble, France

E-mail: `bunau@impmc.upmc.fr`

Abstract. We report the implementation of a fully relativistic time dependent density functional theory (TDDFT) method for the calculation of X-ray absorption spectroscopy in extended systems. It is for the first time that a TDDFT simulation of X-ray absorption in extended systems features a full potential ground state calculation. We prove that this peculiarity of the TDDFT implementation brings undeniable improvement over the previous muffin-tin calculation methods.

PACS numbers: 78.70.Dm, 31.15.A-, 71.10.-w

Submitted to: *J. Phys.: Condens. Matter*

‡ Present adress: IMPMC - 4 place Jussieu, 75005 Paris, France

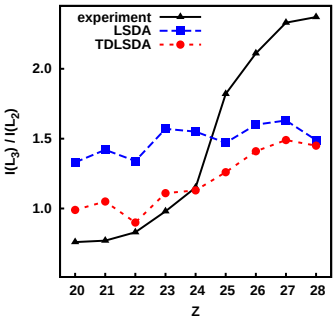

Figure 1. The $L_{2,3}$ branching ratio: the MT - TDLSDA (circles) improves on the one-body LSDA calculations (squares) for the first elements of the $3d$ series. The adiabatic approximation of the TDDFT breaks down when the core hole effect becomes significant, i.e. for the second half of the series. Experimental data (triangles) is taken from ref. [12] and [13] .

X-ray absorption spectroscopy is a very powerful tool in material science, as it probes the electronic and geometrical structures around the absorbing atom. For this spectroscopy, the most common first principles calculation methods are the ones based on density functional theory (DFT) in the one-body approximation [1, 2, 3, 4]. The DFT is actually a ground state theory and often fails to describe the absorption spectra when the probed electronic states are localized, as in the case of $L_{2,3}$ edges of $3d$ elements in various compounds. Such failure suggests the urge of a more advanced treatment of correlations in the description of X-ray absorption spectroscopy. At the current state of the art, the most accurate calculations are those based on the solution of the Bethe-Salpeter equation (BSE) [5]. Nonetheless, they imply a high computational cost that makes BSE calculations not yet suitable for applications at a large scale.

In this article we focus on time dependent density functional theory (TDDFT) [6] as an alternative to BSE for calculations of core spectroscopy. TDDFT introduces a framework particularly suitable for spectroscopy calculations that allows the inclusion of many body effects within reasonable computational cost [7]. Although the TDDFT found lots of applications in quantum chemistry [8], its use in the X-ray frequency range and for extended systems is far less common [9, 10, 11].

Any TDDFT calculation requires the knowledge of the ground state solution and depends on its accuracy. Whereas in real materials non-spherical (i.e. beyond muffin tin) effects are often significant, all existing TDDFT methods for the calculation of X-ray absorption in extended systems rely on the spherical muffin-tin (MT) approximation. In particular, MT approximation assumes that the potential has spherical symmetry within the MT spheres centered on the atoms, and is constant between spheres. We report the implementation of the first TDDFT method that overcomes this limitation. We provide several examples of TDDFT calculations where the agreement with the experimental X-ray absorption spectra is significantly improved by the full potential feature (FP), as compared to its MT counterpart.

In linear response theory (LR) and Hartree units the X-ray absorption cross

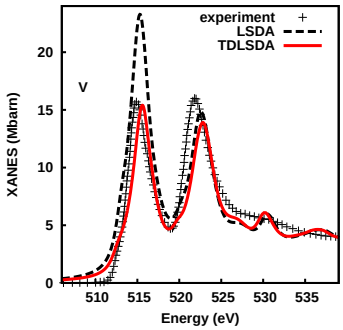

Figure 2. One body LSDA (dashes) and TDLSDA calculations (solid) versus experiment [13] for vanadium at the $L_{2,3}$ edges. Contrary to the LSDA, TDLSDA calculations yield the correct relative peak intensity. All calculations are MT.

section reads [14]:

$$\sigma(\omega) = -\frac{4\pi\omega}{c}\sum_{\sigma\sigma'}\int d^3r \int d^3r' \times \hat{O}^{\dagger}(\omega,\vec{r}\,')\,\Im\chi^{\sigma\sigma'}(\omega,\vec{r},\vec{r}\,')\,\hat{O}(\omega,\vec{r}) \tag{1}$$

with ω the photon energy, σ the spin index and $\hat{O}$ the external field operator. In this article we work within the dipolar approximation $\hat{O} = \vec{\epsilon}\vec{r}$ with $\vec{\epsilon}$ the polarization. In our method, calculations of other terms (quadrupolar, octupolar) are in principle possible, nonetheless these produce no effect for the spectra treated here. Thanks to a Dyson-like equation, the LR-TDDFT allows the description of some many body effects into the linear response function χ of the electron system [7]:

$$\hat{\chi} = (\hat{1} - \hat{\chi}_0\,\hat{K})^{-1}\,\hat{\chi}_0 \tag{2}$$

where $\hat{\chi}_0$ is the ground state response function and $\hat{K}$ the exchange-correlation kernel. In practice, all X-ray absorption TDDFT calculations for extended systems consider a kernel that is local in both space and time (the adiabatic approximation [7]):

$$K^{\sigma\sigma'}(\vec{r},\vec{r}\,',\omega) = \frac{1}{|r-r'|} + f_{xc}^{\sigma\sigma'}(\vec{r},\vec{r}\,',\omega) \tag{3}$$

where the first term is the usual Hartree contribution and the second one is the exchange-correlation contribution in the local spin density approximation (LSDA). In reasonable agreement with ref. [9] we showed that the main contribution to the local kernel is brought by the Hartree term and therefore make no further reference to the choice of the exchange-correlation contribution. All TDDFT calculations presented in this article feature the kernel in eq. 3 (TDLSDA). Let:

$$\phi_g(\vec{r}) = \sum_{\sigma}\phi_g^{\sigma}(\vec{r})\,\zeta_\sigma = \sum_{\sigma} c_{\Lambda_g^\sigma}\,b_g(r)\,Y_{\Lambda_g^\sigma}(\hat{r})\,\zeta_\sigma \tag{4}$$

the wavefunction of the initial, occupied states (index g) corresponding to the resonant transition, where $\Lambda_g^\sigma = (l_g, m_g + \frac{1}{2} - \sigma, \sigma)$ is the set of quantum numbers characterizing the initial states, $c_{\Lambda_g^\sigma}$ the Clebsch-Gordon coefficients and ζ_σ the spin eigenfunction. $b_g(r)$ is the radial wavefunction, which in practice only depends on the

edge corresponding to the initial state g. $Y(\hat{r})$ is standing for the complex spherical harmonics. The final state wavefunction can be written as [15]:

$$\Psi_f(\vec{r},E) = \sum_{\sigma}\sum_{\Lambda_s} a^f_{\Lambda_s}(E)\ \Psi^s_{\Lambda_\sigma}(\vec{r},E)\ \zeta_\sigma \tag{5}$$

Our approach is fully relativistic in the sense that we get the exact solution for the upper component of the wavefunction (with no approximation on the lower component), as described by Wood and Boring [16]. When fully relativistic, the eigenfunctions are the sum of two solutions sharing the same l quantum number but different m [16, 17]. In (5) s is the index over the solution and by convention we take it either $\frac{1}{2}$ or $-\frac{1}{2}$, i.e. the same values as for the spin projection σ. $\Lambda_s = (l, m+\frac{1}{2}-s, s)$ and $\Lambda_\sigma = (l, m+\frac{1}{2}-\sigma, \sigma)$ are sets of quantum numbers describing the final states. $a^f_{\Lambda_s}(E)$ is the amplitude of the Λ_σ contribution to the s component of the final state wavefunction:

$$\Psi^s_{\Lambda_\sigma}(\vec{r},E) = b^s_{\Lambda_\sigma}(r,E)\ Y_{\Lambda_\sigma}(\hat{r}) \tag{6}$$

where $b^s_{\Lambda_\sigma}(r,E)$ is the spin and orbital dependent radial wavefunction. To treat relativistic effects, we solve an exact, effective Schrödinger equation (i.e. rigorously equivalent to the Dirac equation) for both up and down potentials [17].

In order to solve the matrix equation (2) one needs to choose a convenient basis. Following the philosophy of Schwitalla and Ebert [9] and adopted by Ankudinov et al. [11] we consider an expansion of the following kind:

$$\begin{aligned}\chi_0{}^{\sigma\sigma'}(\vec{r},\vec{r}\,',\omega) = &\sum_{gg'}\phi^\sigma_g(\vec{r})\phi^{\sigma'\dagger}_{g'}(\vec{r}\,')\sum_{\Lambda_s\Lambda'_s}\tilde{\chi_0}^{\sigma\sigma'}_{gg',\Lambda_s\Lambda'_s}(\omega)\\ &\times\ \Psi^{s\dagger}_{\Lambda_\sigma}(\vec{r},\omega+E_g)\Psi^{s'}_{\Lambda'_\sigma}(\vec{r}\,',\omega+E_{g'})\delta_{gg'}\end{aligned} \tag{7}$$

as if we were projecting χ_0 on the set of functions formed by the initial state wavefunctions ϕ and the final state ones Ψ. By confronting (7) to the Adler-Wiser expression of χ_0 [9] one obtains the spherical harmonics representation of χ_0:

$$\begin{aligned}\tilde{\chi_0}^{\sigma\sigma'}_{gg',\Lambda_s\Lambda'_s}(\omega) = &-\delta_{gg'}\int_{E_F}^{\infty}\frac{dE}{\pi}\ \frac{\Im\tau_{\Lambda_s\Lambda'_s}(E)}{\omega-(E-E_g)+i\epsilon}\\ &\times\frac{Z^{s'}_{g'\Lambda'_\sigma}(E)\ Z^{s}_{g\Lambda_\sigma}(E)}{Z^{s'}_{g'\Lambda'_\sigma}(\omega+E_{g'})\ Z^{s}_{g\Lambda_\sigma}(\omega+E_g)}\end{aligned} \tag{8}$$

Note that contrary to the previous implementations [9, 11] we calculate χ_0 directly and make no use of the Kramers-Kronig relations. A normalization factor is required in (8), since the set of functions introduced in (7) has a slight energy dependence. Please note the different normalization as compared to the one in ref. [9]. The quantity:

$$Z^s_{g\Lambda_\sigma}(E) = \int_0^R dr\ r^2\ b_g(r)\ b^s_{\Lambda_\sigma}(r,E) \tag{9}$$

is some energy dependent function that is supposed to account for the energy modulations in Ψ. Equation (8) features the multiple scattering matrix τ, whose imaginary part expression is given by the optical theorem [18]:

$$\sum_f\ a^f_{\Lambda'_s}(E)a^{f*}_{\Lambda_s}(E) = -\Im\tau_{\Lambda_s\Lambda'_s}(E) \tag{10}$$

The peculiarity of our method is that the amplitudes $a^f_{\Lambda_s}(E)$ are obtained without any assumption on the form of the scattering potential. The space surrounding the

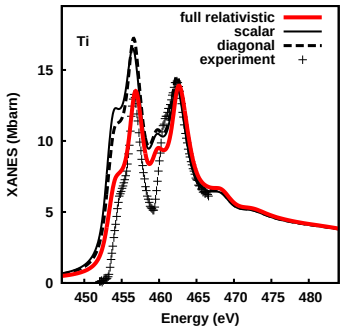

Figure 3. TDDFT calculations of the $L_{2,3}$ edges of titanium: non-relativistic (thin solid), relativistic with TDLSDA kernel forced to be diagonal in spin (dashes), fully relativistic (thick solid). Experimental data (dots) is taken from ref. [12]. The ground state calculation (not shown here) is essentially insensitive to the spin-orbit coupling.

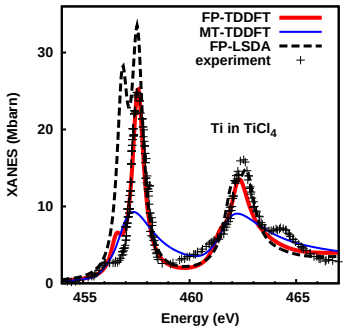

Figure 4. Titanium $L_{2,3}$ edges of the $TiCl_4$ molecules: calculations *versus* experiment [19] (dots). The full potential TDDFT (thick solid) accounts for the sharp features of the experimental spectrum, whereas its MT counterpart (thin solid) fails to. For comparison we show the one-body full potential calculation (dotted line).

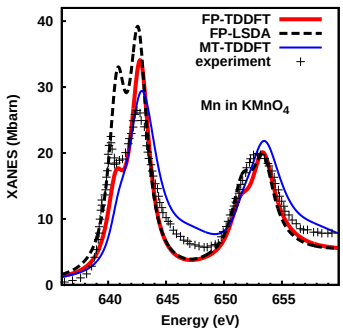

Figure 5. Calculations *versus* experiment [20] (dots) of the $L_{2,3}$ manganese edges in $KMnO_4$. The full potential TDDFT calculation (thick solid) provides better description of the sharp L_3 than its MT counterpart (thin solid).

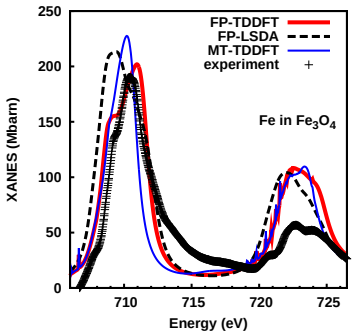

Figure 6. Calculations *versus* experiment [21] (dots) of the $L_{2,3}$ iron edges in the high temperature phase of Fe_3O_4. The full potential TDDFT calculation (thick solid) provides better description of the relative intensities of the two features at L_2 and L_3 edges than its MT counterpart (thin solid). Calculations were scaled at the L_2 edge. The spikes in the MST-TDDFT spectrum are due to numerical issues induced by the denominator in (8).

absorbing atom is discretized and the Dirac equation is solved in every mesh point with no approximation, according to the finite differences method (FDM) [1].

An expansion similar to the one in (7) can be performed on both $\chi^{\sigma\sigma'}(\vec{r},\vec{r}\,',\omega)$ and $K^{\sigma\sigma'}(\vec{r},\vec{r}\,',\omega)$ to obtain the corresponding projections $\tilde{\chi}^{\sigma\sigma'}_{gg',\Lambda_s\Lambda'_s}(\omega)$ and $\tilde{K}^{\sigma\sigma'}_{gg',\Lambda_s\Lambda'_s}(\omega)$, respectively. Therefore the operator Dyson equation (2) becomes a generalized matrix equation, whose dimensions correspond to the σ, g, s, m and l indexes. Finally, the absorption cross section is calculated from eq. 1.

Our method is perfectly able to reproduce the TDDFT (Hartree kernel) results previously reported in literature [9, 11] for closely packed materials. Close packed materials as the pure metals can be calculated accurately in the framework of the multiple scattering theory (MST) relying on the MT approximation. In particular, we calculated the $L_{2,3}$ absorption spectra of pure $3d$ elements (see, for instance, figure 2). Calculations were performed on clusters of 7 Å , i.e. containing some tens of atoms. To compare with results in [9, 11] we define the branching ratio as the ratio between the L_3 and L_2 intensities maxima. In figure 1 we show the evolution of the TDDFT calculated branching ratio throughout the $3d$ series. One can see that the TDDFT effect decreases with the increase of the $2p$ spin-orbit coupling. To understand this behavior, one should mention that the dominant many body effect taken into account by the adiabatic TDDFT is the particle-hole exchange (the inter-edge mixing), whose strength decreases with the increase of the spin-orbit splitting. The remaining disagreement between the calculated branching ratio and the experimental one is due to the effect of the core hole, whose accurate description requires a non-local, frequency dependent exchange correlation kernel. Such kernel does not yet exist. Note that the TDDFT branching ratio for the late $3d$ elements is very close to the one-body result, a consequence of the graduate filling of the d band and of the increased $2p$ spin-orbit coupling.

We found that it is essential to perform fully relativistic calculations for all materials, including the non-magnetic ones. Here, when we oppose relativistic to non-relativistic calculations we refer to the calculation of the final states, *via* an effective Schrödinger equation for the two spins or a usual, scalar Schrödinger equation, respectively. The spin-orbit coupling of the $2p$ is considered under all circumstances.

Our method is essentially different from the one proposed in ref. [11], which assumes that the response function is diagonal in spin. Moreover, we found that the crossed-spin elements $\chi_{\uparrow\downarrow}$, which only appear when the TDDFT calculation is fully relativistic, have a substantial effect even for light materials or when magnetism is not expected (figure 3). On the other hand, whether relativistic or not, we noted that for such materials the ground state is almost the same. This behavior is normal, as the $3d$ orbital moment is quenched by the crystal field, thus the spin-orbit effect is very small. In other words, the crossed-spin elements are negligible in the ground state (in χ_0), while they get enhanced in χ, through the large 2p spin-orbit coupling together with the $2p$-$3d$ exchange coupling described in the kernel. Consequently, we simplified our calculations, which are in principle fully relativistic, by combining a non-relativistic ground state calculation to a fully relativistic TDDFT one. We checked that the emerging result is quasi-identical to the one obtained *via* a complete relativistic calculation scheme. Note that all calculations shown in this article are self-consistent (see the details in [22]) thus two corresponding FP and MT calculations share the same Fermi level.

As stated previously, the main novelty of our method consists in calculating the Kohn-Sham eigenstates with no approximation on the form of the potential. Numerous $3d$ elements compounds benefit from the inclusion of the non-MT effects. A selection of such is to be shown in the following. In all cases, we show the comparison with TDDFT calculations where the Kohn-Sham eigenstates where calculated in MST-MT, where spheres are defined by the intersection of atomic potentials, with an aditional 10 *per* cent overlap. No empty spheres where included in the MST-MT ground state calculation.

The first example concerns the titanium $L_{2,3}$ edges of the $TiCl_4$ molecule (figure 4). The FDM calculation was performed in a 5 Å cluster centered on the molecule and the convolution parameters used are 0.8 and 0.5 for the L_2 and L_3 edge, respectively. In spite of the high symmetry of the absorbing site (T_h), the MT approximation fails to describe the highly localized Ti - Cl bonds. The full potential ground state calculation predicts narrower d-bands than the MST calculated ones, a rather general property of the FDM calculations. Consequently, the corresponding TDDFT scheme brings an undeniable improvement upon the MT approximation.

Oxides are known for the effects of non-sphericity. Consequently, we chose to calculate the manganese edges of $KMnO_4$ (figure 5) and the iron edges of magnetite Fe_3O_4 (figure 6) in both MST-TDDFT and FDM-TDDFT. The calculation clusters contained 36 atoms in the case of $KMnO_4$ and 44 in the one of Fe_3O_4, for both tetrahedral and octahedral iron sites. In all cases, the full potential feature improves the description of the first structure in the L_3 edge. One would expect important non-spherical effects in distorted geometries. Indeed, for $KMnO_4$, the TDDFT calculation disagrees at the position of the mentioned feature, whose presence is related to the tetrahedral distortion of the absorber site. In magnetite, contrary to the MST, full potential TDDFT predicts the good relative intensity between the two features at each edge, an effect that is entirely due to the octahedral contribution. The underestimation of the branching ratio in Fe_3O_4 due to the core hole (2p-3d interaction) that cannot be described within the TDLSDA. For both $KMnO_4$ and Fe_3O_4 the spectral features are sharper at the L_3 edge and rather broad at the L_2. In literature two mechanisms are proposed to explain such differences in the spectral shape: the super Coster-Kronig transition [23] and the charge transfer phenomena [24]. The TDDFT (at least in the adiabatic approximation) calculates neither of them, we therefore performed a distinct

broadening at the two edges (1.7 and 2.2 eV, respectively, for $KMnO_4$, 1 and 1.5 eV for Fe_3O_4) to account for these effects. Generally, the spectral weight of the TDDFT calculations is shifted by some tenths of eV to higher energies from their ground state (LSDA) parent. This shift has been suppressed from the figures and all energy scales were adjusted to the experimental one.

To summarize, we provided several examples of TDDFT calculations benefiting from the full potential feature of the ground state foundation. Any further improvement of the TDDFT calculation should target the TDDFT exchange-correlation kernel, which is beyond the scope of this article. As long as the ground state calculation is concerned, the advancement presented here brings the ground state calculation to the unanimously accepted limitations of the LDA.

[1] Y. Joly. X-ray absorption near edge structure calculations beyond the muffin-tin approximation. *Phys. Rev. B*, 63:125120–125129, 2001.

[2] A. L. Ankudinov, B. Ravel, J. J. Rehr, and S. D. Conradson. Real-space multiple-scattering calculation and interpretation of x-ray-absorption near-edge structure. *Phys. Rev. B*, 58(12):7565–7576, Sep 1998.

[3] D. Cabaret, E. Gaudry, M. Taillefumier, Ph. Sainctavit, and F. Mauri. XANES calculation with an efficient non muffin-tin method: Application to the angular dependence of the Al K-edge in corundum. *Physica Scripta*, T115:131–133, 2005.

[4] H. Ebert. *Electronic Structure and Physical Properties of Solids*, volume 535, page 191. Springer Berlin, 2000.

[5] Robert Laskowski and Peter Blaha. Understanding the $L_{2,3}$ x-ray absorption spectra of early $3d$ transition elements. *Phys. Rev. B*, 82:205104, Nov 2010.

[6] Erich Runge and E. K. U. Gross. Density-functional theory for time-dependent systems. *Phys. Rev. Lett.*, 52(12):997, Mar 1984.

[7] Giovanni Onida, Lucia Reining, and Angel Rubio. Electronic excitations: density-functional versus many-body green's-function approaches. *Rev. Mod. Phys.*, 74(2):601–659, Jun 2002.

[8] G. Fronzoni, M. Stener, P. Decleva, M. de Simone, M. Coreno, P. Franceschi, C. Furlani, and K. C. Prince. X-ray absorption spectroscopy of vocl3, cro2cl2, and mno3cl: An experimental and theoretical study. *The Journal of Physical Chemistry A*, 113(12):2914–2925, 2009.

[9] J. Schwitalla and H. Ebert. Electron Core-Hole Interaction in the X-Ray Absorption Spectroscopy of $3d$ Transition Metals. *Phys. Rev. Lett.*, 80(20):4586–4589, May 1998.

[10] Z. Levine. Magnetic dichroism at the giant dipole resonance of Fe and Mn via time-dependent density-functional theory. *J. Phys. B: At. Mol. Opt. Phys.*, 31:3155–3166, 1998.

[11] A. L. Ankudinov, A. I. Nesvizhskii, and J. J. Rehr. Dynamic screening effects in x-ray absorption spectra. *Phys. Rev. B*, 67(11):115120, Mar 2003.

[12] J. Fink, Th. Müller-Heinzerling, B. Scheerer, W. Speier, F. U. Hillebrecht, J. C. Fuggle, J. Zaanen, and G. A. Sawatzky. 2p absorption spectra of the 3d elements. *Phys. Rev. B*, 32(8):4899–4904, Oct 1985.

[13] Andreas Scherz. Ph.d. disertation in freie universitat berlin. http://www-ssrl.slac.stanford.edu/stohr, 2004.

[14] A. Zangwill and Paul Soven. Density-functional approach to local-field effects in finite systems: Photoabsorption in the rare gases. *Phys. Rev. A*, 21(5):1561–1572, May 1980.

[15] Y. Joly. Interaction matter - polarized light. In E. Beaupaire, H. Bulou, F. Scheurer, and J.P. Kappler, editors, *Magnetism and Synchrotron Radiation*, pages 77–126. Springer, 2010.

[16] J. H. Wood and A. Michael Boring. Improved pauli hamiltonian for local-potential problems. *Phys. Rev. B*, 18:2701–2711, Sep 1978.

[17] Y. Joly, S. Di Matteo, and C. R. Natoli. *Ab initio* simulations of resonant x-ray scattering on the insulating phase of v_2o_3 compared with recent experiments. *Phys. Rev. B*, 69:224401, Jun 2004.

[18] C. R. Natoli, D. K. Misemer, S. Doniach, and F. W. Kutzler. First-principles calculation of x-ray absorption-edge structure in molecular clusters. *Phys. Rev. A*, 22(3):1104–1108, Sep 1980.

[19] A. Wen and A. Hitchcock. Inner shell spectroscopy of (5-c5h5)2ticl2, (5-c5h5)ticl3, and ticl4. *Canadian Journal of Chemistry*, 71(10):1632–1644, 1993.

[20] B. Gilbert, B. H. Frazer, A. Belz, P. G. Conrad, K. H. Nealson, D. Haskel, J. C. Lang, G. Srajer, and G. De Stasio. Multiple scattering calculations of bonding and x-ray absorption spectroscopy of manganese oxides. *The Journal of Physical Chemistry A*, 107(16):2839–2847, 2003.

[21] S. B. Wilkins, S. Di Matteo, T. A. W. Beale, Y. Joly, C. Mazzoli, P. D. Hatton, P. Bencok, F. Yakhou, and V. A. M. Brabers. Critical reexamination of resonant soft x-ray bragg forbidden reflections in magnetite. *Phys. Rev. B*, 79(20):201102, May 2009.

[22] Oana Bunău and Yves Joly. Self-consistent aspects of x-ray absorption calculations. *J. Phys.: Condens. Matter*, 21:345501, 2009.

[23] D. Coster and R. De L. Kronig. New type of auger effect and its influence on the x-ray spectrum. *Physica*, 2(1-12):13 – 24, 1935.

[24] H. Ikeno, F. M. De Groot, E. Stavitski, and I. Tanaka. Multiplet calculations of $L_{2,3}$ x-ray absorption near-edge structures for 3d transition-metal compounds. *Journal of Physics: Condensed Matter*, 21(10), 2009.